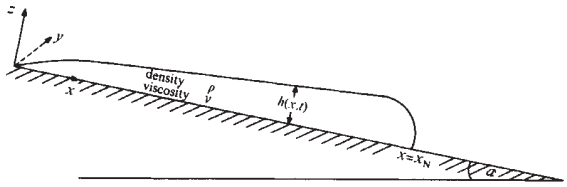

Fig. 2 A sketch of the flow and coordinate system.

tensions indicated that the wavelength is a function of the surface tension. Finally, observations taken during experiments using the same fluid but with amounts differing by up to a factor of 10 indicated that the wavelength is weakly dependent on the initial cross-sectional area A.

The form of the quasi-steady, two-dimensional tip, which is determined by including surface tension and by matching the tip onto the main flow given by equation (7), can be easily determined. The addition to equation (2) of the terms due to surface tension T leads to

$$h_t + (g \sin\alpha/\nu)h^2 h_x - 1/3(T/\rho\nu)h^3 h_{xxxx} = 0 \qquad (8)$$

In the tip the dominant balance is between the second and third terms of equation (8), the solution to which can be written as

$$h = h_N(t)H(\xi) \qquad \xi = (\rho g \sin\alpha/Th_N)^{1/3}(x_N - x) \qquad (9)$$

where $H(\xi)$ satisfies

$$H^3H''' + H^3 = 1 \qquad (10)$$

$$H \to \left(\frac{16}{15}\right)^{1/4} \xi^{3/4} \qquad (\xi \to 0) \qquad (11)$$

$$\to 1 \qquad (\xi \to \infty) \qquad (12)$$

The length scale of the tip is thus given by $(Th_N/\rho g \sin\alpha)^{1/3}$.

The experiments indicated that the instability occurs after the two-dimensional flow has propagated to a critical length X_N^C proportional to $A^{1/2}$. Evaluating the length-scale of the tip at this point and conjecturing that the wavelength, λ, is given, in scale, by this length, suggests that $\lambda \sim (A^{1/2}T/\rho g \sin\alpha)^{1/3}$. The results of the various observations, normalized in this way, are presented in Fig. 4. The data are seen to collapse together systematically with this normalization and are well represented by

$$\lambda = 7.5(A^{1/2}T/\rho g \sin\alpha)^{1/3} \qquad (13)$$

The wavelength remained constant as the amplitude of the instability increased. For the silicone oils, the distance from the origin of the furthest points down the slope increased with time like $t^{0.35}$ while the distance of the minima increased like $t^{0.28}$. For glycerine, the distance of the front of the instability, once well established, increased like $t^{0.6}$ while the minima were virtually stationary.

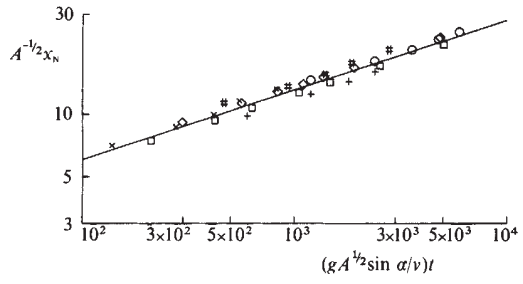

Fig. 3 The length of the two-dimensional flow, normalized with respect to $A^{1/2}$, as a functon of a suitably non-dimensional time. The straight line is the theoretical prediction obtained from equation (7). The experimental points are for values of ν, $\sin\alpha$, A in cgs units of: □, 12.9, 0.093, 8.9; ◇, 12.9, 0.20, 3.1; ○12.9, 0.65, 5.9; +, 9.8, 0.20, 9.0; ×, 9.8, 0.15, 3.6; #, 1.2, 0.11, 1.0.

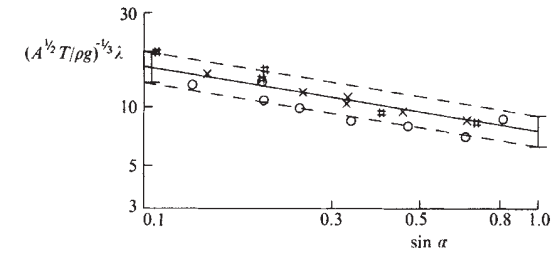

Fig. 4 The wavelength of the instability at the front, normalized with respect to $(A^{1/2}T/\rho g)^{1/3}$, as a function of the slope angle, α. Experiments with fluids of viscosities 12.9, 9.8 and 1.2 cm^2s^{-1} are plotted as ○, × and # respectively. The solid line is given by equation (14) and is the best-fit to the data. The two error bars at the end of the line represent ±15%, a typical standard deviation of the wavelength across the slope. Where two or more data points fell on top of each other all but one were omitted for the sake of clarity.

I thank E. J. Hinch for stimulating and helpful conversations, many other of my colleagues in DAMTP for useful discussions, J. M. Wheeler for experimental help and for preparation of the figures, and D. C. Cheesley, D. Lipman, G. Parker and E. J. Sharp for technical assistance.

Received 14 June; accepted 8 September 1982.

1. Huppert, H. E. *J. Fluid Mech.* **121**, 43–58 (1982).
2. Huppert, H. E. *et al. J. Volcan. Geotherm. Res.* **14** (in the press).
3. Batchelor, G. K. *An Introduction to Fluid Dynamics* (Cambridge University Press, 1967).
4. Hocking, L. M. *Q. Jl Mech. appl. Math.* **34**, 37–55 (1981).

Forces between two adsorbed polyethylene oxide layers immersed in a good aqueous solvent

Jacob Klein*† & Paul Luckham*

* Cavendish Laboratory, Madingley Road, Cambridge CB3 0HE, UK
† Polymer Department, Weizmann Institute, Rehovot, Israel

Recent measurements of the forces acting between two polystyrene layers adsorbed onto mica surfaces, immersed in a poor solvent for the polymer, show strong initial attraction as the surfaces approach, followed by ultimate repulsion[1]. This has been attributed to attractive osmotic interactions between the adsorbed layers, and possibly to the effect of bridging[2,3]. We have extended these measurements to the case of polyethylene oxide (PEO) layers adsorbed on mica, immersed in an aqueous 0.1 M KNO_3 medium at *p*H 6 (a good solvent for PEO). Using monodispersed polymer of two molecular weights, we find that an equilibrium force–distance profile is indicated. As the surfaces bearing the adsorbed PEO approach, repulsive forces commence at a surface separation $D \simeq 6 \pm 1 R_g$ (unperturbed radius of gyration of the respective polymers) and increase monotonically on approach; on subsequent separation the forces decrease monotonically to zero. We find no evidence for attraction or adhesion between the adsorbed layers in this system.

The experimental technique and procedure closely resemble those previously described[1,4]. The method permits the measurement of the force $F(D)$ acting between the mica surfaces a distance D apart, as well as the mean refractive index $n(D)$ of the medium separating them.

The forces were first determined between the bare mica surfaces in pure electrolyte. Polyethylene oxide solution was

0028–0836/82/480429—03$01.00

then added to the required concentration (either 10^{-5} or 1.5×10^{-4} g ml^{-1}), and the surfaces left to incubate for 16 ± 2 h. Forces were then measured both in compression and decompression at different intervals (1 min to 1 h) and at various approach and separation rates (15–60 min per cycle), following which the PEO solution was replaced by pure solvent, and measurements repeated. The overall duration of experiments was generally between 48 and 72 h.

The PEO samples used were obtained from Toyo Soda (Japan). They were anionically prepared and their molecular characteristics (manufacturers data, determined by GPC) are shown below.

	M_w	M_w/M_n	R_g
PEO1	4.00×10^4	1.03	6.5 nm
PEO2	1.60×10^5	1.04	13 nm

The results are shown in Fig. 1. In the pure electrolyte (Fig. 1*a*) the forces between the mica surfaces are typical of electrostatic double-layer (DLVO) interactions[4], with a secondary minimum as indicated in the inset and the characteristic strong short range repulsion (Fig. 1*a*). The surface potential of the mica deduced from the Debye length is ~100 mV. The force–distance profiles as well as the surface potential correspond closely to those observed previously for mica surfaces in various aqueous electrolytes[4].

Following adsorption of the polymer, the force profiles change as shown in Fig. 1*a*: no forces are observed as the surfaces approach from $D\simeq500$ nm down to $D\simeq6\pm1\ R_g$ (corresponding to 35–40 nm for PEO1, 65–75 nm for PEO2), and thereafter monotonically increasing repulsion sets in. The surfaces were generally brought in to about 6 ± 1 nm separation. The shape of $F(D)$ on decompression and recompression of the surfaces depends to some extent on the rate at which these are carried out: if decompression is rapid (up to about 5 min for separation to $F(D)=0$) the dashed curve (Fig. 1*a*) is followed. However, if separation is sufficiently slow (30–60 min for separation to $F(D)=0$), the decompression curve merges (within error) into the original compression profile (solid curve). A similar effect is observed on recompression: if the surfaces are compressed, then rapidly separated, (<5 min) and then brought together again within 5 min, then the resulting $F(D)$ profile on subsequent compression follows the broken curve. If a longer time (30–60 min) elapses between separation and approach, the compression profile reverts to the original solid curve. Thus the variation of $F(D)$ with compression–decompression rates in these experiments is within the shaded regions indicated. We find no evidence for the build-up of thick adsorbed layers with time beyond the values corresponding to the solid curves in Fig. 1. The results described were obtained (within experimental error) for the two incubation concentrations used, both in solution and following the replacement of polymer solution by pure electrolyte. They suggest that there is a quasi-equilibrium force–distance profile for this system, represented by the solid curves, while the broken curves indicate the effect on $F(D)$ as a result of incomplete relaxation of the adsorbed polymeric layers at short times ($\lesssim5$ min).

Figure 1*b* shows the variation of refractive index $n(D)$ with surface separation D for PEO1. These values of $n(D)$ were measured both in compression and decompression, and were the same (within error) both in solution and following the replacement of solution by pure electrolyte, at the two incubation concentrations. They indicate (as for polystyrene adsorbed onto mica from cyclohexane) that there is little desorption or extrusion of polymers over the times and in the conditions of our experiments. The adsorbance Γ of polymer onto the mica may be estimated from $n(D)$ (ref. 1), and corresponds to $\Gamma\simeq5$ mg m^{-2} of mica surface. To our knowledge there are no independent measurements of PEO adsorbance onto plane surfaces to compare this value of Γ with, though we note that it is comparable to adsorbance values for other polymers on plane surfaces[5]. It is, however, higher than PEO adsorbance onto colloidal silica particles[6] (for which $\Gamma\sim1$ mg m^{-2}).

The onset of interactions between the adsorbed layers in the present study suggests an effective extension of polymer from each mica surface of some $3R_g$. This compares with values of $\sim2R_g$ measured for various polymers (but not PEO) adsorbed on plane surface from θ-solvents[7], and with an effective extension of some $1.5\ R_g$ for polystyrene adsorbed onto mica in worse-than θ conditions[1]. Our value of 2.5–$3R_g$ is comparable with a hydrodynamic thickness of about $2R_g$ for PEO layers adsorbed onto polystyrene latex particles in a good aqueous solvent, as measured by light scattering[8], and also with theoretically predicted values of some $3R_g$ for adsorbed poly-

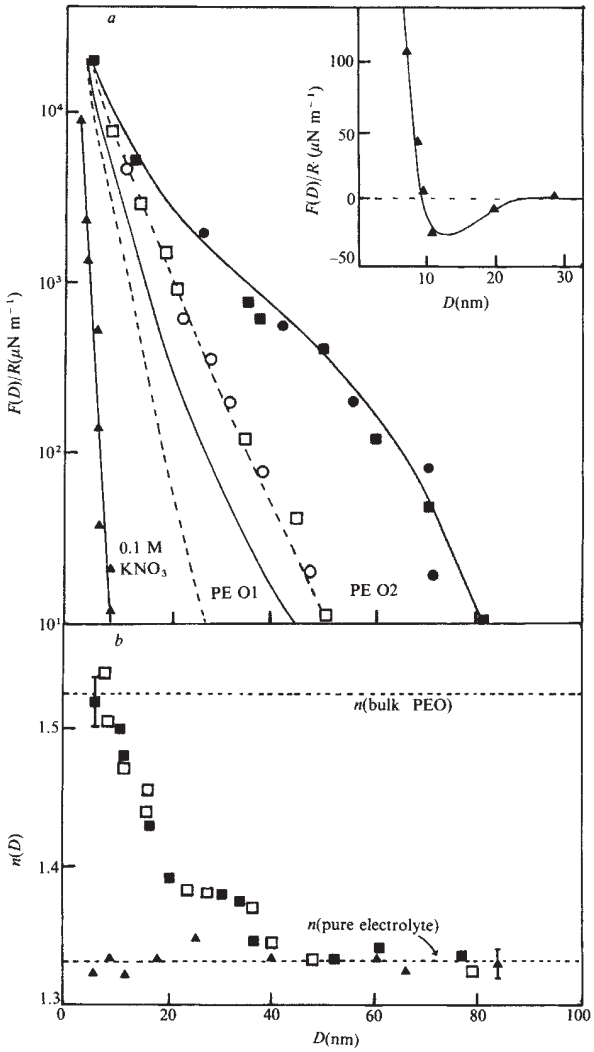

Fig. 1 *a*, Forces $F(D)$ between curved mica surface (mean radius of curvature $R\simeq0.5\times10^{-2}$ m) in 0.1 M KNO_3 (BDH Analar grade, in de-ionized double-distilled water) at 20 ± 2 °C. ▲, Force profile in pure electrolyte. The inset shows the secondary minimum on a linear scale. PEO2: Forces $F(D)$ following 16 ± 2 h immersion in 1.5×10^{-4} g ml^{-1} PEO2 solution. ■, Compression of surfaces following prolonged (>60 min) separation. □, Compression ~5 min after rapid decompression of surfaces. ●, Slow decompression. ○, Rapid decompression. Intermediate rates fall in shaded region. See text for details. PEO1: Forces $F(D)$ following 16 ± 2 h immersion in PEO1 solutions. Solid line, compression after prolonged (>60 min) separations; also slow decompression. Dashed line, rapid decompression. Both the pure electrolyte and the polymer solutions were filtered (0.22 μm Millipore) before use. *b*, Mean refractive index $n(D)$ of medium separating mica surfaces. ▲, in 0.1 M KNO_3; ■, following 16 ± 2 h incubation in 10^{-5} g ml^{-1} PEO1 solution; □, following incubation in PEO1 solution and the subsequent replacement of the solution by pure electrolyte. Values unchanged over 24 h.

mers in an athermal solvent[4]. The monotonically repulsive nature of the interactions suggests that for this system there is little effect of bridging or desorption (which could lead to attraction)[2,9], the forces being due to an increasingly repulsive osmotic interaction as the opposing polymer layers come into overlap in the good solvent[2,3,9].

Our results contrast with the earlier study by Israelachvili and co-workers, who used a similar method to measure $F(D)$ between mica surfaces in an aqueous solution of highly polydisperse PEO[10] (Carbowax resin WSR N80, Union Carbide). Their investigation indicated the continuous buildup with time of progressively thicker layers of surface adsorbed material (up to 1,000 nm over 24 h), as well as complex short- and long-time hysteretic behaviour suggestive of gel-like material on the surfaces. This may be due to the polydisperse nature of the polymer, as well as the possible presence of microgels or trace chemical impurities in the as-received Carbowax Resin (ref. 11 and J. N. Israelachvili, personal communication).

The present findings indicate that the interactions between adsorbed layers of monodispersed PEO across a good aqueous solvent are monotonically repulsive, and may be represented by a quasi-equilibrium force–distance profile at times longer than ~1 h. The extension of the adsorbed layers from each surface is somewhat larger than corresponding, independently measured values for polymers on plane surfaces in θ-solvents; the refractive index data indicates (in accordance with previous studies) a quasi-irreversible adsorption of polymer onto the mica surface.

We thank Professor D. Tabor for interest and helpful discussions, and Dr J. N. Israelachvili for useful suggestions.

Received 15 July; accepted 14 October 1982.

1. Klein, J. *Nature* **288**, 248–250 (1980); *JCS Faraday I* (in the press).
2. Scheutjens, J. M. H. M. & Fleer, G. J. *Adv. Colloid Interface Sci.* **16**, 361–381 (1982).
3. Klein, J. & Pincus, P. *Macromolecules* **15**, 1129–1135 (1982).
4. Israelachvili, J. N. & Adams, G. E. *JCS Faraday I* **74**, 975–1101 (1978).
5. Grant, W. H., Smith, L. E. & Stromberg, R. R. *Disc. Faraday Soc.* **59**, 209–217 (1976).
6. Rubio, J. & Kitchener, J. A. *J. Colloid Interface Sci.* **57**, 132–142 (1976).
7. Stromberg, R. R., Tutas, D. J. & Passaglia, E. *J. phys. Chem.* **69**, 3955–3964 (1965).
8. Barnett, K. G. *et al. Polymer* **22**, 283–284 (1981).
9. De Gennes, P. G. *Macromolecules* **15**, 492–500 (1982).
10. Israelachvili, J. N., Tandon, R. K. & White, L. R. *Nature* **277**, 120–121 (1979); *J. Colloid. Interface Sci.* **78**, 432–446 (1980).
11. Union Carbide WSR-N80 Product Specification: 1-44K N80-1a, 70320 00, 19-6-1979.

Magnetostratigraphical dating of loess deposits in China

Friedrich Heller

Institut für Geophysik, ETH-Hönggerberg, CH-8093 Zürich, Switzerland

Liu Tung-sheng

Institute of Geology, Academia Sinica, PO Box 634, Beijing, China

The age of Chinese loess deposits has long been disputed. Biostratigraphical and earlier magnetostratigraphical investigations placed the entire loess formation within the Pleistocene. The new palaeomagnetic measurements reported here on a bore hole section near Lochuan (Shaanxi province) suggest a clearly defined magnetic polarity zonation which extends below the Olduvai subchron. A late Pliocene age of ~2.4 Myr is assigned to the oldest loess sediments measured. The intensity variations of natural remanent magnetization (NRM) and low field magnetic susceptibility are indicative of climatic changes during loess deposition.

In northern China nearly half a million square kilometres are covered by loess sediments. Along the middle Huangho valley these wind-transported, yellow to red-brown sediments occupy a coherent area of more than 300,000 km^2, known as the loess plateau[1]. Here the loess deposits generally approach a thickness of 80–120 m. Typically they consist of an alternation of (1) silty loess layers which developed in cold and arid climatic conditions and (2) clayey loess or palaeosoil beds which are indicative of warm and humid climate (see Fig. 1: succession of loess- and soil(S)-horizons). Some of the soil horizons are developed in such a way that they can be recognized and correlated over large distances. They serve as stratigraphical marker horizons[2]. The environmental variations during loess formation are documented by faunal changes, especially of snail assemblages[3], by the degree of crystallization of clay minerals[4], and by carbonate content and other geochemical indicators[5].

On the basis of lithology, unconformable contacts and erosion surfaces the loess deposit has been subdivided into three main stratigraphical units[6–9] which all have been assigned a Pleistocene age: The Malan Loess of late Pleistocene age, The middle Pleistocene Lishih Loess and the early Pleistocene Wucheng Loess (Fig. 1). The biostratigraphical age estimates have been supported by several palaeomagnetic investigations[10–12]. According to remanent magnetization directions obtained after alternating field (a.f.) demagnetization, the Brunhes–Matuyama boundary has been found to coincide roughly with the Wucheng–Lishih transition. The Jaramillo subchron was identified in the middle of the Wucheng division, thus the oldest strata were estimated to have an age of <1.2 Myr.

We have sampled a long core from a bore hole near Lochuan (Shaanxi province) ~800 km south-west of Beijing (lat. 35.4 °N; long. 109.5 °E) for palaeomagnetic analysis. The core penetrates a 136-m thick loess sequence which has been deposited on top of an Upper Pliocene (Hipparion bearing) lateritic substratum. More than 230 samples were obtained from the core with an average sampling interval of 60 cm. The samples were oriented relative to the vertical but not azimuthally. Before demagnetization the NRM intensity is relatively strong with a mean value of 5.08×10^{-2} Am^{-1} for 150 soil samples, and 2.26×10^{-2} Am^{-1} for 181 loess samples. The low field susceptibility of the soil horizons (mean: 2.49×10^{-3} SI units) also is about twice that of the loess layers (mean: 1.16×10^{-3} SI units). High field experiments show that the main magnetic minerals are magnetite and haematite. The NRM is strongly affected by secondary, viscous remanent magnetization (VRM) so that the NRM vector always gives inclinations consistent with the present field of the Earth. Advantage was taken of this property to detect several misoriented (inverted) samples. Because major portions of viscous magnetization (up to 80% of total NRM) are removed by low a.f.s of the order of 10–15 mT, the VRM apparently resides mainly in magnetite. However, viscosity tests in the laboratory show that progressive a.f. demagnetization increases the instability of NRM. A.f. cleaning of NRM often results in rather erratic or badly defined demagnetization curves. Thermal demagnetization also removes a large secondary VRM component up to 200 °C, but above 300 °C a well defined and stable component is observed which has either positive or negative inclination depending on the stratigraphical position. On orthogonal vector plots this characteristic component decreases undirectionally towards the origin of projection on further heating. Maximum unblocking temperatures are usually above 575 °C. Thus the characteristic remanent magnetization of the loess is probably carried by haematite. Details of the loess rock magnetic properties will be described elsewhere.

After thermal demagnetization at 350 °C the core is subdivided into several clearly defined polarity zones, separated by sharp transitions (Fig. 1). In contrast to the results of earlier investigations which were based on a.f. cleaned NRM directions[10–12], the positive and negative inclinations average vectorially to the absolute value of the present local geomagnetic field inclination ($I = 52.5°$). From top to bottom of the core the polarity changes are correlated with: (1) the Brunhes–Matuyama boundary at core depth 53.05 m; (2) the Jaramillo subchron between 67.30 and 72.50 m; (3) the Olduvai subchron between 107.40 and 113.10 m.

No definite evidence of shorter term geomagnetic excursions is indicated in our data. Three samples (out of a total of 231)

0028–0836/82/480431—03$01.00